Electronic Supplementary Material (ESI) for Chemical Communications

A Face-capped $[Fe_4L_4]^{8+}$ Spin Crossover Tetrahedral Cage

Alan Ferguson,[1] Marie A. Squire,[1] Diana Siretanu,[2,3] Dmitri Mitcov,[2,3] Corine Mathonière,[4,5] Rodolphe Clérac,*[,2,3] Paul E. Kruger*[,1]

[1] Department of Chemistry, University of Canterbury, Private Bag 4800, Christchurch, 8041, New Zealand.

[2] CNRS, CRPP, UPR 8641, F-33600 Pessac, France.

[3] Univ. Bordeaux, CRPP, UPR 8641, F-33600 Pessac, France.

[4] CNRS, ICMCB, UPR 9048, F-33600 Pessac, France.

[5] Univ. Bordeaux, ICMCB, UPR 9048, F-33600 Pessac, France.

Supplementary Information

Materials and Methods

All reagents were used as received without further purification from BDH and Sigma Aldrich.

The TGA was carried out on an Alphatech SDT Q600 TGA/DSC apparatus. The sample holder was alumina crucible and it was heated at 1 degree/min under a nitrogen flow of 100mL/min.

^{1}H and ^{13}C NMR spectroscopy was carried on a Varian INOVA 500 spectrometer operating at 500 MHz for ^{1}H and 126 MHz for ^{13}C or an Agilent 400 MR spectrometer operating at 400 MHz for ^{1}H and 376 MHz for ^{19}F.

High resolution mass spectra were recorded with a Bruker maXis 3G UHR-TOF mass spectrometer.

Infrared spectra were recorded on a Perkin Elmer Spectrum One FTIR spectrometers in the range 400-4000 cm^{-1}. Samples were analyzed via diffuse reflectance in ground KBr.

Elemental analyses (C, H, N) were conducted at Campbell Microanalytical Laboratories, Otago University, Dunedin.

UV-vis. spectra were recorded between 350 and 650 nm using a Varian Cary 5000 UV-vis recording spectrophotometer. Variable temperature UV-vis data were obtained using an Oxford Liquid Nitrogen Cryostat Optistat^{ON} (static) equipped with an Oxford ITC^{502} controller operating between 77 and 300 K. Solutions were prepared from crystals of **1** dissolved in acetone at a concentration of $1.06 \cdot 10^{-4}$ mol/L.

Reflectivity measurements were performed on a home-built CRPP reflectivity apparatus using freshly filtered compounds. This set-up collects reflected light from the sample (that is the sum of direct and diffuse reflected light) and operates between 10 and 300 K over spectrometric range of 400 - 1000 nm. The light for spectrometry is a halogen-tungsten light source (Leica CLS 150 XD tungsten halogen source adjustable from 0.5 mW/cm^2 to 1 W/cm^2). The measurements were calibrated relative to a NIST traceable reflectance standard (sphere Optics, ref SG3054).

Magnetic susceptibility measurements were carried out on a Quantum Design SQUID magnetometer MPMS-XL (CRPP) operating between 1.8 and 400 K for applied dc fields ranging from -7 to 7 T. Measurements in solid state were performed on a microcrystalline sample of **1** (19.57 mg) that was filtered from its mother liquor and dried in air less than 2 minutes prior to its introduction at 200 K in the magnetometer. The dried compound was obtained from **1** after a period of 24 h at 100°C (8.57 mg). These solid samples were introduced in polyethylene bags (3 × 0.5 × 0.02 cm) for measurements. Experiments in acetone solutions were carried out in sealed plastic straws under argon with concentration of $1.3 \cdot 10^{-4}$ mol/L. The chosen concentration for the magnetic measurements was determined after multiple tests down to 77 K to avoid precipitation of powder and/or crystals during cooling down. An *M* vs *H* measurement was systematically performed at 100 K to confirm the absence of ferromagnetic impurities. Magnetic data was corrected for the sample holder and diamagnetic contributions for all magnetic measurements. In figure 2, the following equation deduced from ideal solution model[S1, S2] was used:

$$\chi T = \chi T_{LS} + \frac{\chi T_{HS} - \chi T_{LS}}{1 + \exp\left(\frac{\Delta H}{R}\left(\frac{1}{T} - \frac{1}{T_{1/2}}\right)\right)}$$

with χT_{LS} and χT_{HS} being the χT product for **1** in its low-spin and high-spin state respectively. It is worth noting that the χT_{HS} value was fixed in the fitting procedures at 13 cm^3 K/mol to help the fitting convergence. Keeping free this parameter leads to non-physical value of χT_{HS}. As expected, the obtained χT_{LS} values were all very close to zero.

Photomagnetic measurements were performed using a halogen-tungsten light source (Leica CLS 150 XD tungsten halogen source adjustable from 0.5 mW/cm^2 to 1 W/cm^2) coupled through an optical fibre directed into the magnetometer cavity. 2.7 mg samples were packed into a thermoformed plastic straw placed about 3.5 cm from the optical fibre.

Synthesis of 2,4,6-tris(4-nitrophenoxy)triazine:

This synthesis was adapted from a previous synthetic procedure.[S3] To a stirred solution of cyanuric chloride (1.5 g, 8.2 mmol) in acetone (100 mL) was added slowly a solution of *p*-nitrophenol (3.00 g, 25.2 mmol) and NaOH (1.00 g, 25.2 mmol) in H_2O (100 mL) and acetone (20 mL) with gentle cooling. When the two solutions had been combined the mixture was heated to reflux overnight to give a white crystalline product. The product was collected by filtration and washed with H_2O (3 × 20 mL) and MeOH (3 × 20 mL) before being dried under vacuum to give 2,4,6-tris(4-nitrophenoxy)triazine as a white crystalline solid: (3.65 g, 91%). MP 209-211 °C; ^{1}H NMR (500 MHz, $CDCl_3$): δ 8.30 (2H, d, J = 9 Hz), 7.33 (2H, d, J = 9 Hz); ^{13}C NMR (126 MHz, $CDCl_3$) δ 119.5, 126.5, 144.5, 160.9; m/z (HR-ESI-MS): 493.0739 ([M+H$^+$] $C_{21}H_{13}N_6O_9$ requires 493.0739).

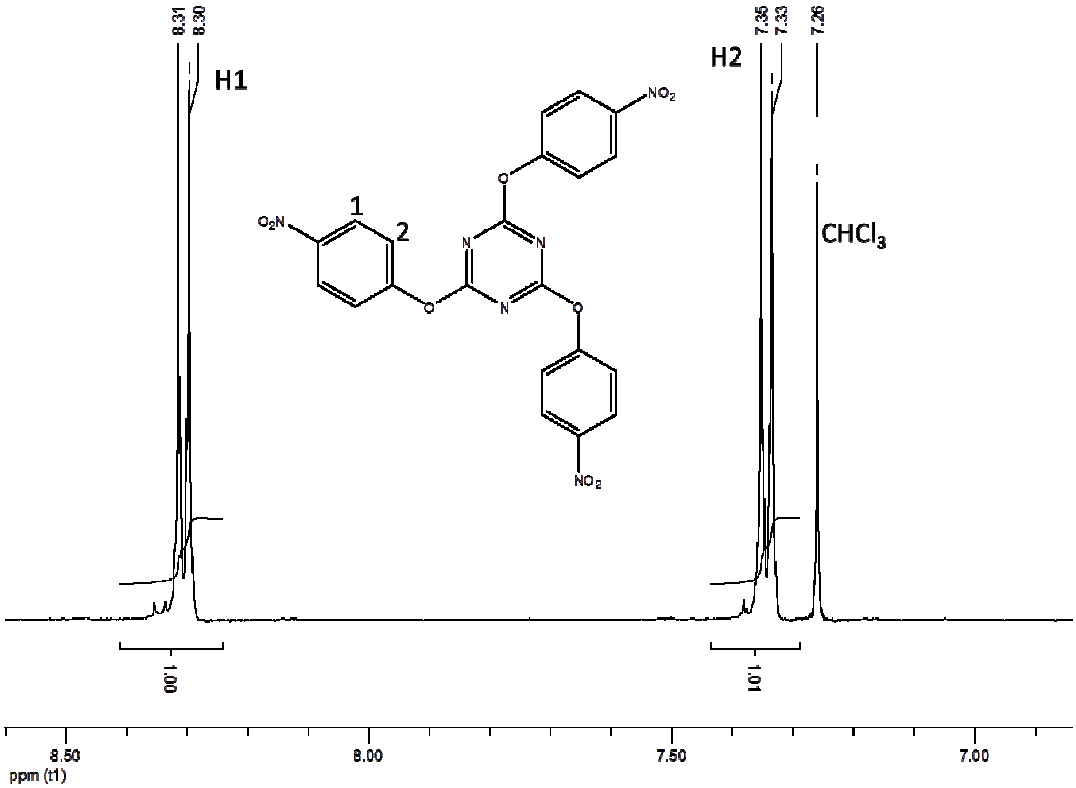

Fig. S1. ^{1}HNMR spectrum (500 MHz, $CDCl_3$) of 2,4,6-tris(4-nitrophenoxy)triazine with peak assignment.

Synthesis of 2,4,6-tris(4-aminophenoxy)triazine:

To a stirred solution of 2,4,6-tris(4-nitrophenoxy)triazine (3.55 g, 7.3 mmol) in EtOAc (140 mL) under inert atmosphere was added slowly Pd/C 10% (0.36 g, 3.4 mmol). Once all Pd/C 10% had been added the mixture was placed under a H_2 atmosphere and stirred at room temperature overnight. The mixture was filtered to remove the Pd/C 10% to give a clear solution. The solvent was removed under reduced pressure to give a residue which was washed with diethyl ether (3 × 50 mL) to give 2,4,6-tris(4-aminophenoxy)triazine as a white powder (2.55 g, 87%). MP 226-228 °C; ^{1}H NMR (500 MHz, $CDCl_3$): δ 6.92 (2H, d, J = 9 Hz), 6.62 (2H, d, J = 9 Hz), 3.62 (2H, s); ^{13}C NMR (126 MHz, $CDCl_3$): δ 114.1, 121.7, 141.8, 146.8, 173.8; m/z (HR-ESI-MS) 403.1522 ([M+H$^+$] $C_{21}H_{19}N_6O_3$ requires 403.1513).

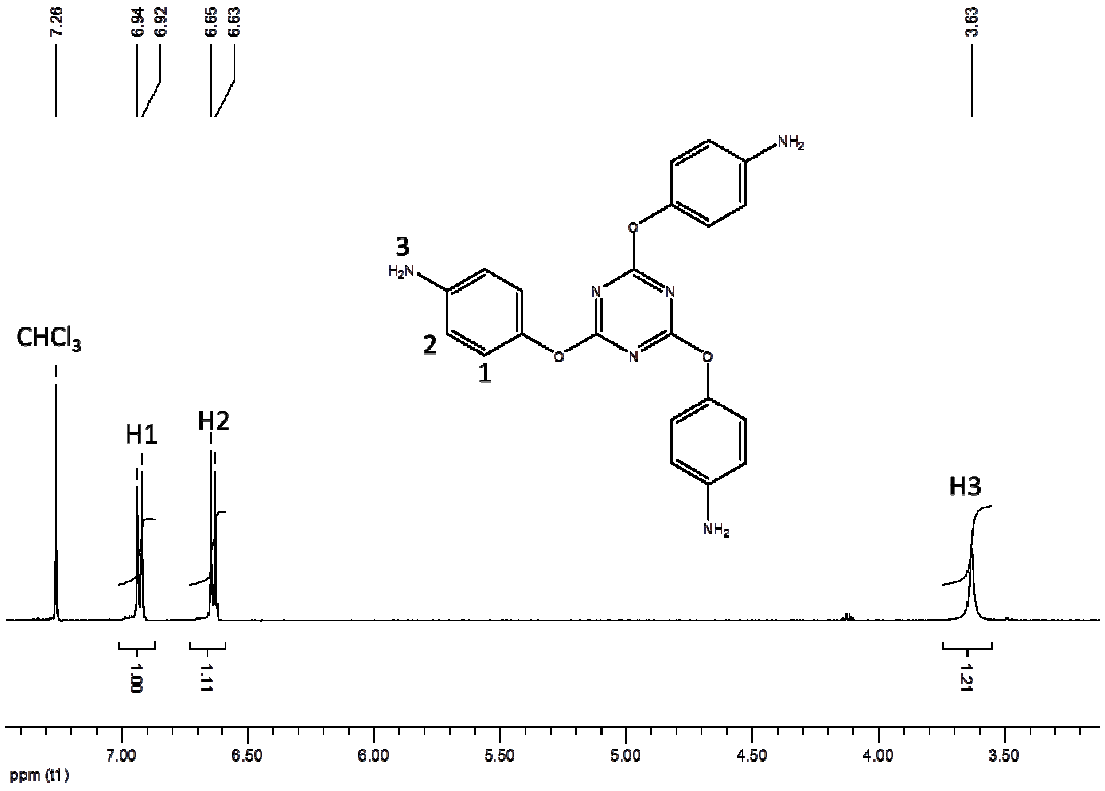

Fig. S2. ^{1}HNMR spectrum (500 MHz, $CDCl_3$) of 2,4,6-tris(4-aminophenoxy)triazine with peak assignment.

Synthesis of $\{[Fe_4L_4](BF_4)_8 \cdot 14.75MeCN \cdot 4.5C_6H_6 \cdot 3H_2O\}$: 1

To a stirred solution of 2,4,6-tris(4-aminophenoxy)triazine (25.0 mg, 0.062 mmol) in MeCN (15 mL) was added 2-imidazole-carboxaldehyde (17.9 mg, 0.186 mmol) and $Fe(BF_4)_2 \cdot 6H_2O$ (20.9 mg, 0.062 mmol). The mixture was stirred at ~50 °C for 20 mins to give a dark red/purple solution. Vapor diffusion of benzene into the reaction solution yielded large rod-like crystals of **1** (35 mg, 55% yield). Sample dried at 80 °C under vacuum gave the following elemental analyses: Found C, 44.85; H, 3.13; N, 19.14 %; $C_{132}H_{96}N_{48}O_{12}Fe_4B_8F_{32} \cdot 3H_2O$ requires C, 45.05; H, 2.92; N 19.11 %. m/z (HR-ESI-MS): 475.9287 $[BF_4+Fe_4L_4 - H]^{6+}$; 570.9130 $[BF_4+Fe_4L_4 - 2H]^{5+}$; 713.3896 $[BF_4+Fe_4L_4 - 3H]^{4+}$; 950.8503 $[BF_4+Fe_4L_4 - 4H]^{3+}$; ν_{max}/cm^{-1} (KBr): 3642 s, 3038 br, 2922 br, 1569 (s, C=N), 1497 s, 1436 s, 1369 s, 1201 s, 1084 (s, BF_4^-), 889 m, 859 m.

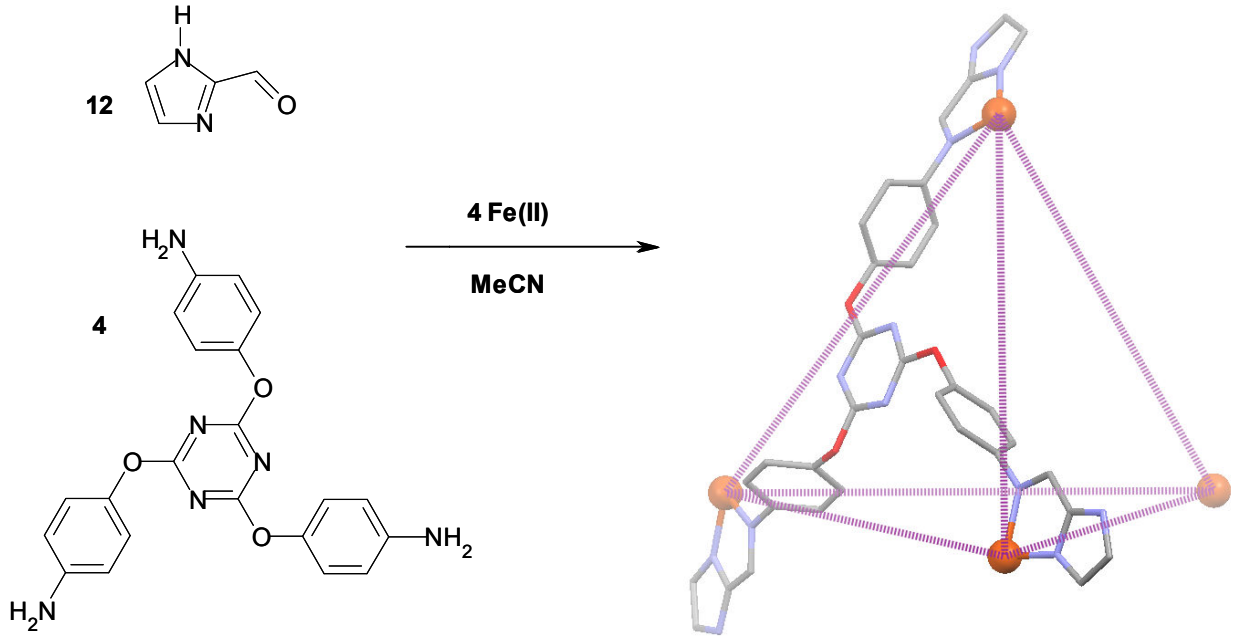

Fig. S3. Subcomponent self-assembly of $[M_4L_4]^{8+}$ tetrahedral cage from 2,4,6-tris(4-aminophenoxy)triazine, 2-imidazolecarboxaldehyde and $Fe(BF_4)_2$ in acetonitrile to yield the corresponding face-capped tetrahedron.

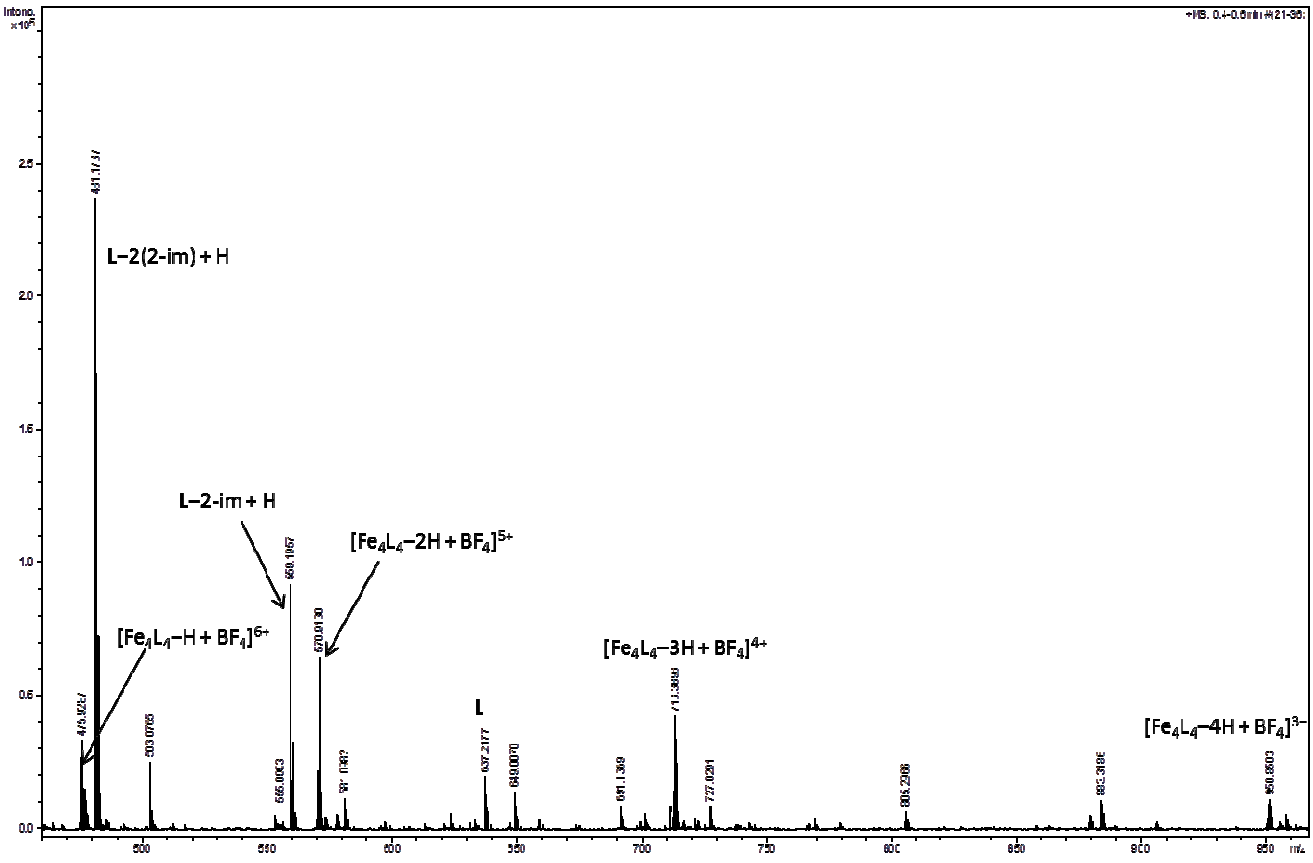

Fig. S4. ES Mass Spectrum of **1** with peak assignment.

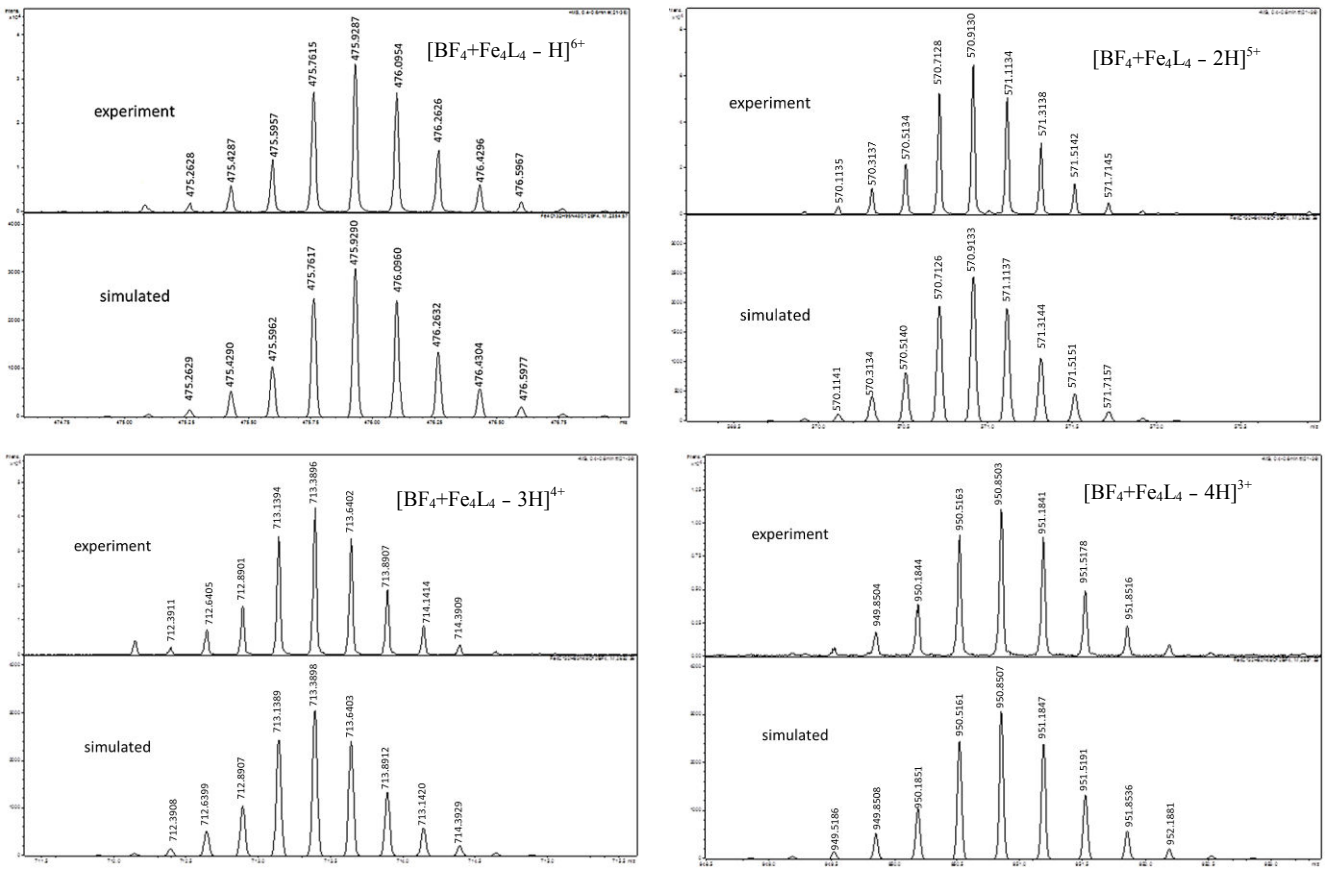

Fig. S5. ES Mass Spectra of **1** showing the experimental and simulated isotope peak patterns for the $[BF_4+Fe_4L_4 - H]^{6+}$; $[BF_4+Fe_4L_4 - 2H]^{5+}$; $[BF_4+Fe_4L_4 - 3H]^{4+}$; and $[BF_4+Fe_4L_4 - 4H]^{3+}$ cations, respectively.

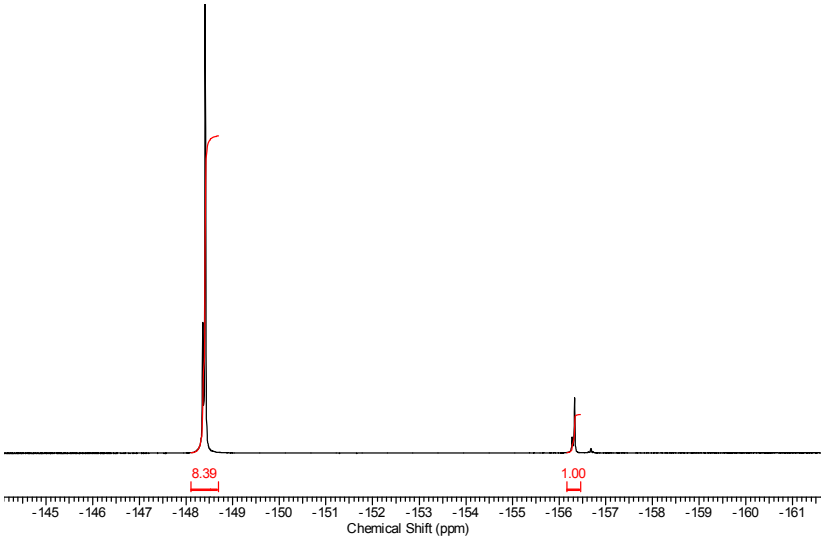

Fig. S6. ^{19}F NMR for **1** showing the two environments for the $[BF4]^-$ ions. [d_6-acetone, 25 °C].

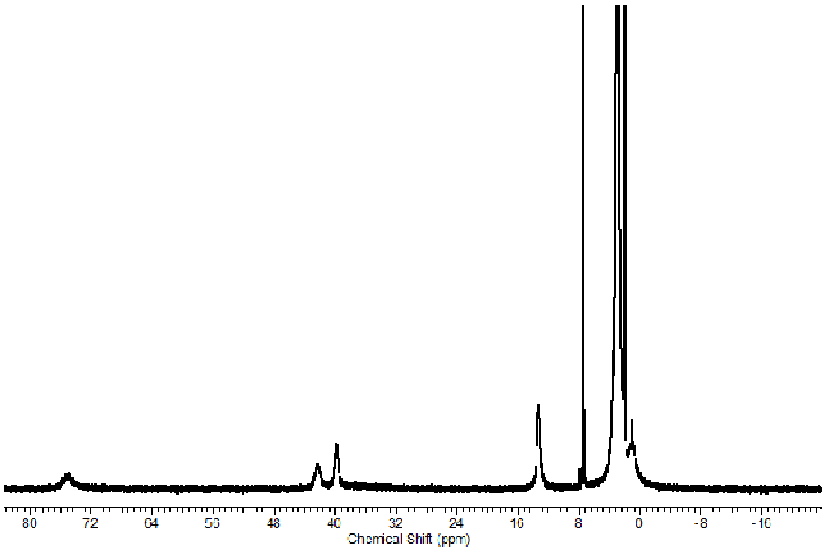

Fig. S7. ^{1}H NMR for **1** showing peak broadening consistent with the presence of HS Fe(II). [d_6-acetone, 25 °C].

X-ray structural characterization of $\{[Fe_4L_4](BF_4)_8 \cdot 14.75MeCN \cdot 4.5C_6H_6 \cdot 3H_2O\}$, 1:

The structural analysis at 153 K was performed on a rotating anode Rigaku Spider with monochromated Cu-*Ka* (λ = 1.54178 Å) radiation. CrystalClear[S4] was used for the data collection and FSProcess[S5] was used for the data processing. The structure was solved using direct methods with SHELXS[S6] and refined on *Olex2*[S7] using all data by full matrix least-squares procedures with SHELXL-97.[S8] Multi-scan absorption correction using ABSCOR.[S9] Hydrogen atoms were included in calculated positions with isotropic displacement parameters 1.2 times the isotropic equivalent of their carrier atoms. All but one of the external $[BF_4]^-$ anions were restrained (DFIX) to follow the tetrahedral geometry expected for BF_4 and their thermal parameters were constrained to be roughly equal (EDAP). The benzene solvent molecules and one imidazole group (N6 C7 N8 C9 C10) were restrained (FLAT) to be planar. The geometries of the MeCN solvent molecules were restrained to chemically reasonable bond lengths. All solvent molecules and all but one of the $[BF_4]^-$ anions were refined isotropically. The remaining residual electron density was not modelled and the SQUEEZE protocol inside PLATON[S10] was used to remove the void electron density (total of 272 electrons per unit cell). These were assigned as 3 MeCN, 2 benzene and 12 water molecules per unit cell (0.75 MeCN, 0.5 benzene, 3 H_2O per cage), which is in agreement with the microanalysis results obtained. The structural analysis at 293 K was performed on an Agilent dual wavelength SuperNova with monochromated Mo-*Ka* (λ = 0.71070 Å) radiation. CrysAlisPro[S11] was used for the data collection and data processing. The structure was solved using direct methods with SHELXS[S6] and refined on *Olex2*[S7] using all data by full matrix least-squares procedures with SHELXL-97.[S8] Multi-scan absorption correction using SCALE3 ABSPACK.[S12] Hydrogen atoms were included in calculated positions with isotropic displacement parameters 1.2 times the isotropic equivalent of their carrier atoms. The crystals were mounted and sealed in a glass capillary containing a small amount of the mother liquor. Unfortunately Cu radiation could not be used for the data collection due to absorption by the capillary. The use of Mo radiation resulted in weaker data than that collected at 153 K despite a crystal of similar size and quality being diffracted. Several crystals were diffracted to find the crystal with the strongest diffraction. A full set of data was collected; however, the high angle data was dominated by noise and was omitted. All of the external $[BF_4]^-$ anions were restrained (DFIX) to follow the tetrahedral geometry expected for BF_4 and all of the $[BF_4]^-$ anions had their thermal parameters constrained to be roughly equal (EDAP). All $[BF_4]^-$ anions were also refined isotropically. Several of the imidazole groups had their thermal parameters constrained to be roughly equal (EDAP). The remaining residual electron density was not modelled and the SQUEEZE protocol inside PLATON[S10] was used to remove the void electron density (total of 2237 electrons per unit cell). These were assigned as 73 MeCN, 12 benzene and 12 water molecules per unit cell (18.25 MeCN, 3 benzene, 3 H_2O per cage), which is in reasonable agreement with the structure at 153 K.

Table S1. Crystal data for $[Fe_4L_4](BF_4)_8$, 1, at 153 and 293 K

	153 K	293 K
empirical formula	$C_{188.5}H_{173.25}N_{62.75}O_{15}Fe_4B_8F_{32}$	$C_{198.5}H_{185.75}N_{66.25}O_{15}Fe_4B_8F_{32}$
formula weight	4475.53	4657.26
temperature	153(2) K	293(2) K
wavelength	1.54178 Å	0.71070 Å
crystal system, space group	monoclinic, *C*2/*c*	monoclinic, *C*2/*c*
volume	22681(3) $Å^3$	23864(5) $Å^3$
Z	4	4
calculated density	1.274 g cm^{-3}	1.007 g cm^{-3}
absorption coefficient	2.809 mm^{-1}	0.314 mm^{-1}
crystal size	0.21 × 0.18 × 0.08 mm	0.25 × 0.12 × 0.08 mm
unit cell dimensions	a = 46.2462(8) Å	a = 46.627(7) Å
	b = 15.5937(3) Å β = 123.814(9)°	b = 15.8882(13) Å β = 127.15(2)°
	c = 37.854(3) Å	c = 40.415(5) Å
$\theta_{min,\ max}$	6.52, 65.08	2.58, 20.82
limiting indices	$-54 \le h \le 54$, $-17 \le k \le 18$, $-44 \le l \le 44$	$-46 \le h \le 46$, $-15 \le k \le 14$, $-40 \le l \le 40$
N/ N_{ind}	100797/19209 (R_{int} 0.1007)	31491/12411 (R_{int} 0.1507)
reflns/paramaters/restraints	19209/1170/85	12411/894/78
$T_{min,max}$	0.425, 1.000	0.274, 1.000
GoF	1.557	0.919
final R indices $[I > 2\sigma(I)]^a$	$R_1(F)$ 0.1416, $wR_2(F^2)$ 0.4335	$R_1(F)$ 0.1270, $wR_2(F^2)$ 0.3563
$\Delta\rho_{min,max}$	-0.853, 1.731 $e^-Å^{-3}$	-0.430, 0.760 $e^-Å^{-3}$

[a] $R_1 = \Sigma(|F_o|-|F_c|)/\Sigma(|F_o|)$; $wR_2 = [\Sigma\{w(F_o^2-F_c^2)^2/\Sigma\{w(F_o^2)^2\}]^{1/2}$

Table S2. Comparison of Fe-N bonds lengths in 1 at 153 and 293 K

153 K	$Fe-N_{imidazole}$ (Å)		$Fe-N_{imine}$ (Å)	
Fe1	N1	1.952(5)	N17	1.990(5)
	N6	1.964(5)	N22	2.013(5)
	N15	1.961(5)	N45	2.003(5)
Fe2	N76	1.975(6)	N70	1.980 (6)
	N77	1.942(6)	N83	2.017(6)
	N89	1.956(6)	N95	2.005(6)
293 K				
Fe1	N13	1.969(11)	N3	2.087(10)
	N21	1.979(9)	N4	2.053(10)
	N50	1.926(7)	N24	2.088(8)
Fe2	N7	2.047(11)	N8	2.101(9)
	N78	1.979 (7)	N10	2.118(10)
	N80	2.051(11)	N131	2.074(13)

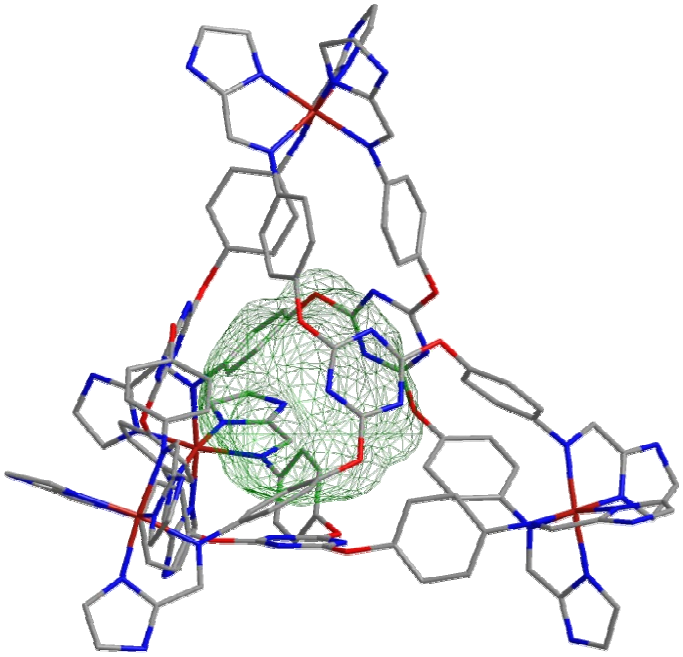

Fig. S8. Image of the internal cavity/void volume (green mesh) of $[Fe_4L_4]$ (at 153 K) with encapsulated $[BF_4]^-$ anion removed generated by Chem3D Ultra 10.0.[S13] Calculated as 106 $Å^3$ by PLATON VOIDS.[S14]

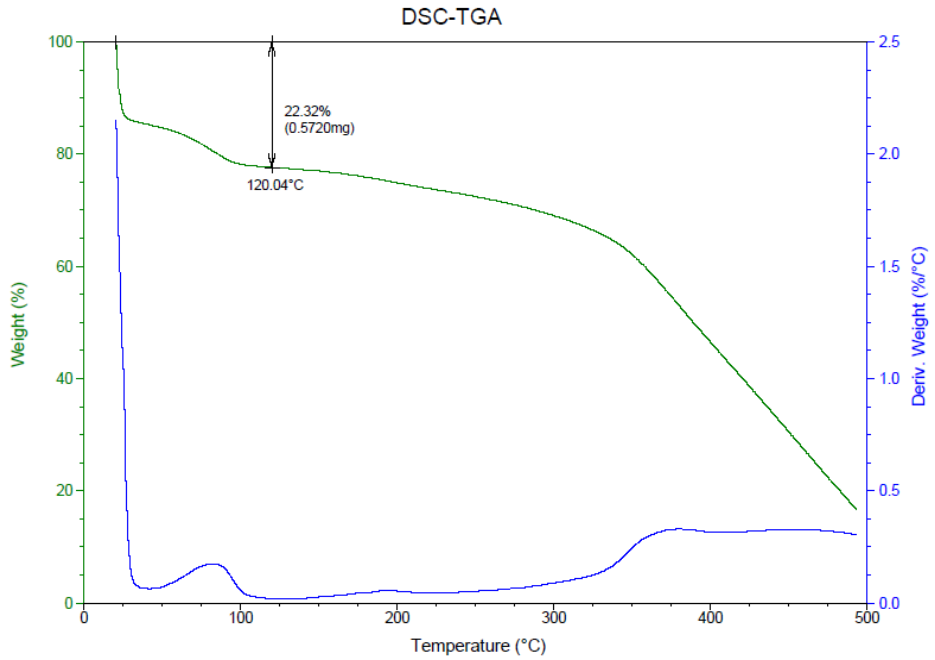

Fig. S9. Thermo-gravimetric analysis (TGA) of **1**. The analysis of the curve for **1** reveals significant and immediate weight loss of *ca.* 13 % at 25 °C consistent with the loss of the lattice MeCN molecules (calc. 13.5 %), followed by further gradual weight loss of *ca*. 9.3 % between 25 < *T* < 120 °C, consistent with loss of the benzene and water molecules (calc. 9.05 %). The desolvated phase gradually loses weight from 120 < *T* < 300 °C where after complex decomposition occurs.

Optical reflectivity and photomagnetic measurements performed upon 1.

Optical reflectivity measurements on **1** were performed on a polycrystalline sample (filtered a few minutes before measurements) under a weak white light irradiation of about 0.05 mW/cm^2 and a scanning temperature rate of 4 K/min. When the temperature decreases from 250 K down to 50 K, there is a slight increase in the near IR component while the visible component remains largely the same. Below 50 K there is slight decrease in the reflectivity in the near IR region (Figure S10).

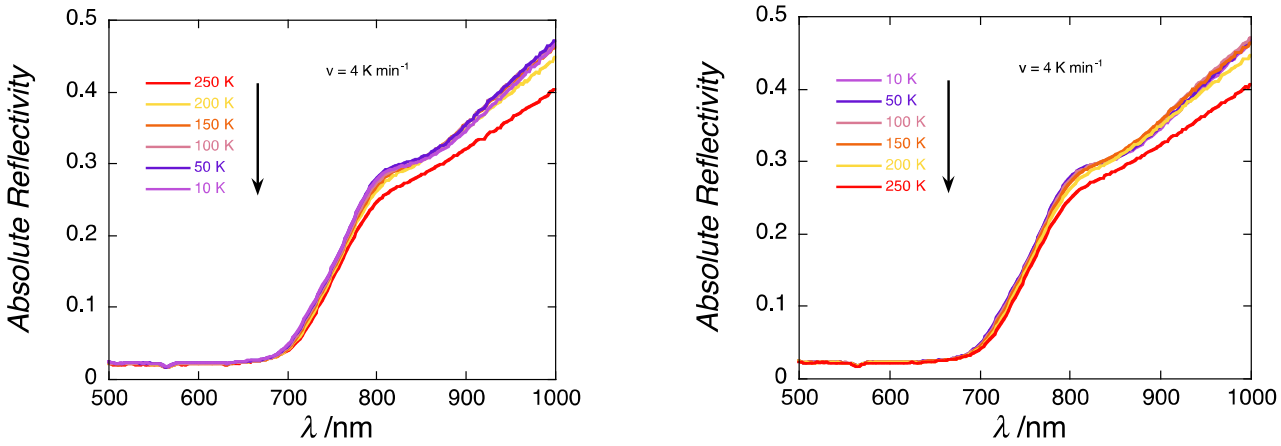

Fig. S10. Optical reflectivity measurements of **1** under weak white light irradiation (0.05 mW/cm^2) and a scanning temperature rate of 4 K/min decreasing the temperature between 250 and 10 K (**left**) and increasing the temperature between 10 and 250 K (**right**).

As shown in Figure S10, the observed thermal behaviour is completely reversible. An alternative way to visualize the spectra thermal variation is to consider the thermal dependence of the reflectivity at 900 ± 5 nm (Figure S11). Upon cooling from 250 K, the reflectivity gradually increases to a value at 0.354 down to 150 K before remaining almost constant to 50 K. This behaviour is a signature of the thermal spin crossover phenomenon seen already by magnetic measurements. Below 50 K, it decreases slightly to a value of 0.344 suggesting a small photo-induced effect for **1**. Upon increasing the temperature from 10 K, the reflectivity increases up to 0.354 at 70 K as a signature of the small photo-induced effect of the Fe(II) centres. Between 70 and 150 K, the reflectivity is almost constant before again gradually decreasing to 0.321 at 250 K. These reflectivity measurements show that the compound, in its low spin-state, is only slightly sensitive, probably on the sample surface, to the white light irradiation.

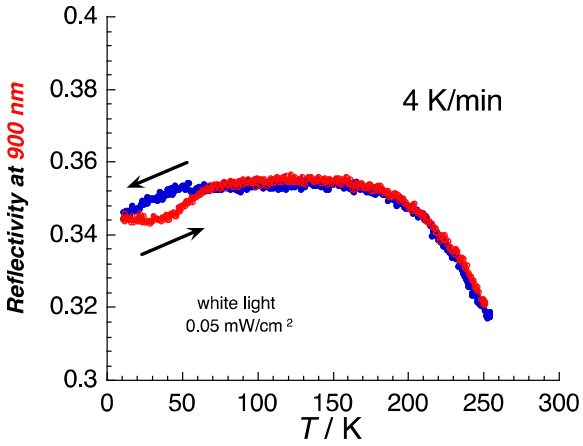

Fig. S11. Thermal dependence of the reflectivity at 900 nm in cooling (blue) and heating (red) modes under weak white light irradiation (0.05 mW/cm^2) and a scanning temperature rate of 4 K/min.

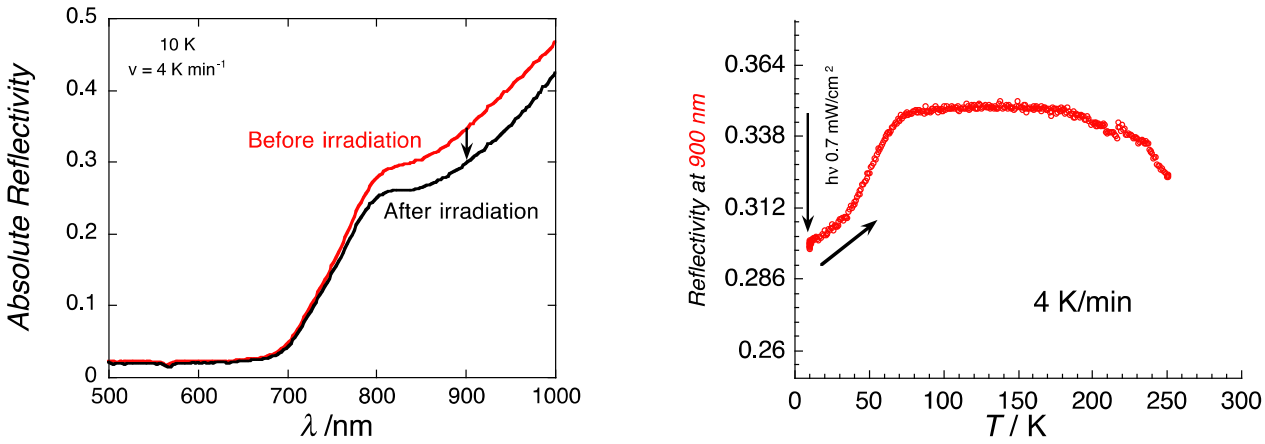

Fig. S12. Left: Optical reflectivity measurements of **1** under weak white light irradiation (0.05 mW/cm^2) at 10 K before (red) and after (black) a 12 hours white light irradiation of the sample with 0.7 mW/cm^2. **Right**: Temperature dependence of the absolute optical reflectivity (heating mode) at 900 nm under weak white light irradiation (0.05 mW/cm^2) after irradiation at 10 K with white light (P = 0.7 mW/cm^2) for 12 hours.

To probe and eventually optimize the photo-excitation yield, additional measurements were performed at 10 K, with the sample exposed to stronger and longer white light irradiations. At 10 K after 12 hours of irradiation at 0.7 mW/cm^2 (Figure S12) a marked decrease of the optical reflectivity is observed in the near IR region while the visible region remains the same. At 900 nm, the optical reflectivity decreases from 0.34 to 0.30 after irradiation. When the temperature is increased, an increase in the reflectivity is observed up to 0.35 at 75 K. Between 75 K and 150 K the reflectivity remains constant before, as previously seen, a gradual decrease of the optical reflectivity down to 0.32 at 250 K due to the thermal spin-crossover of this compound. Even after optimization of the photo-excitation, the photo-conversion of the LS_4 state to the HS_4 state remains very incomplete and probably effective only at the surface of the sample. Therefore the optical reflectivity measurements suggest that the compound is probably very poorly photomagnetic below ~70 K. This assumption was checked at low temperatures measuring the magnetic susceptibility before and after white light irradiation within a MPMS magnetometer. As suggested by the optical reflectivity measurements, a small photomagnetic effect is observed under white light (2 mW/cm^2) at 10 K (left part of Figure S13). The χT product at 10 K starts at 0.13 cm^{3}K/mol and increases to around 0.46 cm^{3}K/mol after 17 hours under white light irradiation. After this white light irradiation the χT *vs* T data were measured (right part of Figure S13). When increasing the temperature, the χT product increases from 1.8 K to 20 K as a signature of the well-known magnetic anisotropy of Fe(II) HS species. Above 20 K, the χT product begins to decrease until at around 60 K it returns to follow the χT vs T curve measured in the dark. The exact

same behaviour is observed when irradiated under red light (647 nm, 2 mW/cm^2) at 10 K. These results confirm a very small photomagnetic effect for **1** that is probably limited to the surface or a small volume near the surface of the sample.

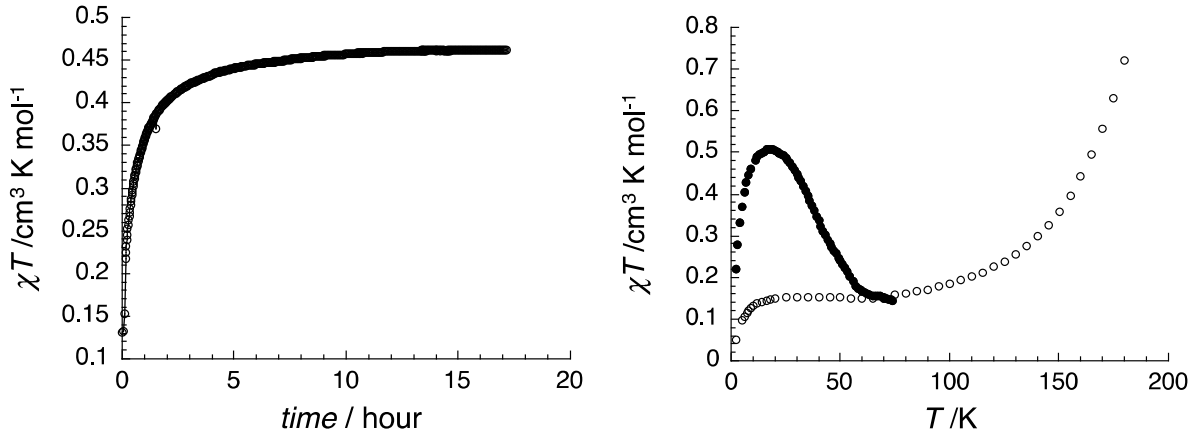

Fig. S13. **Left:** Time dependence of the χT product (with χ defined as the molar magnetic susceptibility and equal to M/H) for compound **1** at 10 K and 0.5 T under white light irradiation with P = 2 mW/cm^2. **Right:** Temperature dependence of the χT product in the dark before irradiation (open dots), and after irradiation (closed dots, white light with P = 2 mW/cm^2, at 0.4 K/min) at 1 T.

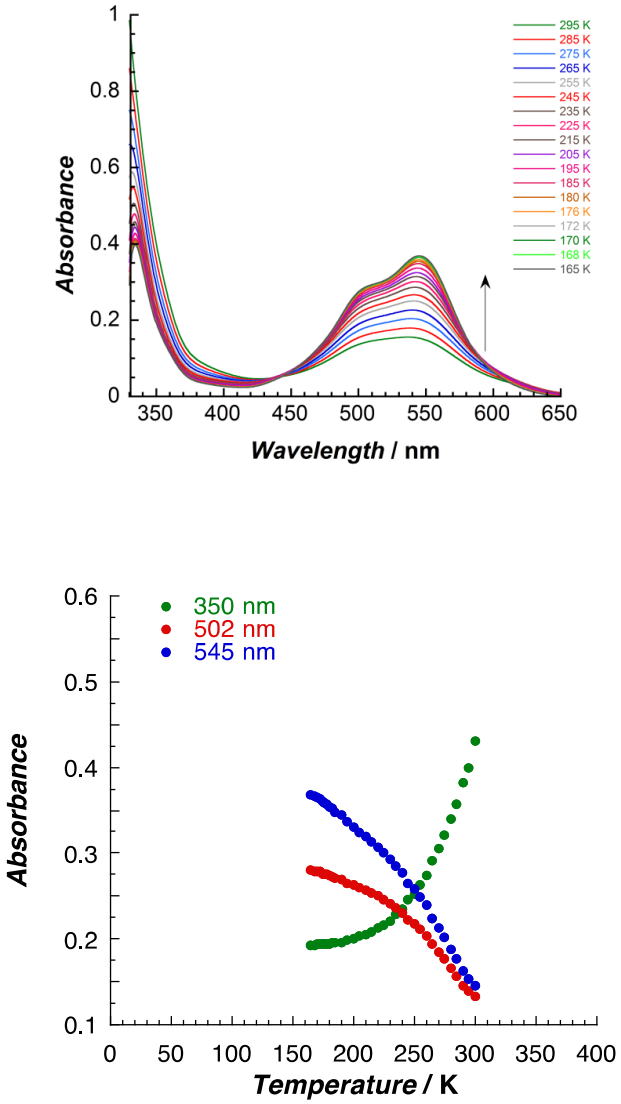

Fig. S14. UV-vis. spectra for $[Fe_4L_4]^{8+}$, **1**, in acetone in cooling mode (at 0.2 to 0.3 K/min) from 295 K to the freezing point of the solution (**top**) and temperature dependence of the solution absorbance at 350, 502 and 545 nm (**bottom).**.

Acknowledgments:

We thank Prof. D. Bassani (Bordeaux 1 University) for the access to the UV-vis. spectrometer, and Assoc. Prof. S. Telfer and Prof. G. Jameson (Massey University, NZ) for assistance with the crystallography.

References:

(S1) P. Atkins, J. De. Paula, *Physical Chemistry.*, 8th Edition, 2006, Ed. Oxford University Press, Chapter 5.

(S2) O. Kahn, *Molecular Magnetism*, VCH, 1993, 60.

(S3) F. C. Schaefer, J. T. Thurston and J. R. Dudley, *J. Am. Chem. Soc.*, 1951, **73**, 2990-2992.

(S4) *CrystalClear: An Integrated Program for the Collection and Processing of Area Detector Data*, Rigaku Corporation. 2005.

(S5) *FS Process*, Rigaku Corporation. 1998.

(S6) G. M. Sheldrick, *Acta Cryst., Sect. A: Fundam. Crystallogr.*, 1990, **46**, 467.

(S7) O. V. Dolomanov, L. J. Bourhis, R. J. Gildea, J. A. K. Howard and H. Puschmann, *J. Appl. Cryst.*, 2009, **42**, 339.

(S8) G. M. Sheldrick, *Acta Cryst.*, 2008, **A64**, 112-122.

(S9) T. Higashi, *ABSCOR*, Rigaku Corporation. 1995.

(S10) A. L. Spek, *PLATON, A Multipurpose Crystallographic Tool*, Utrecht University, Utrecht, The Netherlands, 2008.

(S11) CrysAlisPro, Agilent Technologies, Version 1.171.35.19

(S12) CrysAlisPro, Agilent Technologies, Version 1.171.35.19; Empirical absorption correction using spherical harmonics, implemented in SCALE3 ABSPACK scaling algorithm.

(S13) CambridgeSoft, *Chem3D Ultra 10.0*, 2006.

(S14) PLATON VOIDS probe diameter 1.2 Å, grid 0.2 Å; A. L. Spek, *J. Appl. Crystallogr.,* 2003, **36**, 7-13.